Design and Color Response of Colorimetric Multilumophore Oxygen Sensors

Rachel C. Evans[*,†,‡] **and Peter Douglas**[†,⊥]

Department of Chemistry, Swansea University, Singleton Park, Swansea SA2 8PP, U.K.

ABSTRACT The preparation of multilumophore colorimetric luminescent oxygen sensors exhibiting red−green, red−blue, and red−green−blue color space responses across oxygen partial pressures in the range of 0−760 Torr is described. We show how the relative lumophore concentration, emission lifetime, and permeability of the polymer host matrix to oxygen may be used to control both the color space response and the sensitivity of these sensors, thus enabling the device to be optimized for operation over a specific oxygen concentration range or application. The Commission Internationale de L'Éclairage (CIE) *xy* color space response and oxygen sensitivity of these experimental multilumophore sensors has been modeled using a combination of CIE color coordinates and Stern−Volmer quenching kinetics, and generally good agreement between the experimental and modeled response is obtained. This approach will therefore provide a useful preexperimentation tool for the design of sensors with specific response characteristics.

KEYWORDS: oxygen sensor • luminescence • colorimetric • CIE *xy* color coordinates

INTRODUCTION

Over the past decade, optical oxygen sensors, based on the principle of luminescence quenching of an immobilized lumophore by molecular oxygen, have revolutionized oxygen detection in many technological applications, for example, imaging oxygen concentration gradients in biological samples (1−3), monitoring the integrity of modified atmosphere food packaging (4−6), and measuring surface air pressure distributions on aerodynamic models in wind tunnels using pressure-sensitive paints (7−13).

Various sensor designs have been proposed, some of which are available as commercial products (14). The basic device structure consists of an oxygen-sensitive lumophore, typically a ruthenium(II) polypyridyl complex (2, 15−19) or platinum(II) or palladium(II) porphyrin (15, 20−23), encapsulated or dispersed in a thin oxygen-permeable film (e.g., polymer (18, 19, 21−23), sol−gel (17, 24), or hybrid (2, 16) material). Most workers determine the luminescence quenching from intensity or lifetime measurements and relate it to the oxygen concentration using a Stern−Volmer analysis. In recent years, several useful advances have been made in sensor design and detection. First, light-emitting diodes have become a cheap and common excitation source for optical sensors (16, 24−29). Second, multilumophore sensors, incorporating a second or even third sensing element, thus enabling self-referencing and correction for excitation and temperature fluctuations, have become commonplace (8−13, 30). Finally, portable detection systems, for example, lifetime imaging cameras, are now commercially available, opening the door for optical sensing in the field (27). However, for many applications, qualitative or semiquantitative oxygen determination is often all that is required. To meet this demand, we recently reported the first colorimetric luminescent oxygen sensors with a "traffic-light" response, where the sensor response is indicated by a shift in the sensor emission color from red to green upon exposure to oxygen (31, 32). This color-change technology eliminates the need for expensive photodetection systems when only a semiquantitative measurement of the oxygen concentration is required. Other groups have successfully adopted our original approach, producing colorimetric oxygen sensors using different host matrices (e.g., alumina) (33) or different color-contrasting lumophores (e.g., quantum dots) (34), showing that our initial proof of principle is both reproducible and versatile.

However, the design of such colorimetric sensors is not trivial. The sensor response, in terms of both the color space and detection range, is dependent upon several factors, including the emission spectra of the lumophores, the relative absorption and emission efficiency of each lumophore at the excitation wavelength, absorption of emission by any overlying lumophores, and the relative sensitivity of each lumophore/polymer combination to oxygen quenching. Thus, a theoretical approach to preexperimentation sensor design is crucial if reproducible sensors for practical applications are to be produced. Herein we report the design and development of some practical examples of two- and three-lumophore colorimetric oxygen sensors, which exhibit either a red−green, red−blue, or red−green−blue color change response. Our studies show how the relative lumophore concentration, emission lifetime, and permeability of the polymer host matrix to oxygen may be used to control the color space response of these sensors. We apply a theoretical model based on CIE *xy* color coordinates (35),

* Corresponding author. E-mail: rachelcevans@yahoo.co.uk.
Received for review January 6, 2009 and accepted March 11, 2009
† Department of Chemistry.
‡ Current address: Department of Chemistry, University of Coimbra, Rua Larga, 3004-535 Coimbra, Portugal and Department of Physics, CICECO, University of Aveiro, 3810-193 Aveiro, Portugal.
⊥ Current address: Chemistry Group, School of Engineering, Swansea University, Singleton Park, Swansea SA2 8PP, U.K.
DOI: 10.1021/am900007m

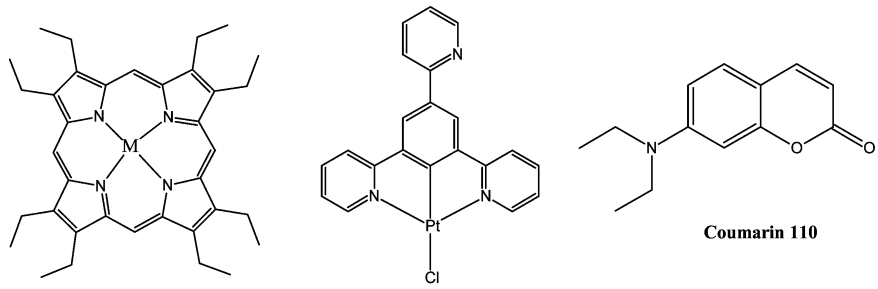

FIGURE 1. Lumophore structures.

Table 1. Extinction Coefficients at 380 nm (ϵ_{380}), Emission Maxima (λ_{em}), Emission Quantum Yields (Φ_{em}), Emission Lifetimes (τ), Stern−Volmer Quenching Constants (k^{SV}), and Color Coordinates (xy) for the Lumophores Used in This Study

L	ε_{380} [mol dm^3 cm^{-1}]	λ_{em} [nm]	Φ	T [μs]	k^{SV} [Torr^{-1}]	xy
PtOEP	290 000[a]	647 (red)[a]	0.40[a]	~100[a]	0.196[e]	0.70, 0.31
PdOEP	79 700[b]	660 (red)[a]	0.20[a]	~990[a]	3.475[e]	0.71, 0.29
Ptpyr	6 900[c]	506 (green)[c]	0.57[c]	~9.2[c]	0.007[f]	0.25, 0.64
C110	30 200[d]	425 (blue)[d]	0.60[d]	~0.0024[d]	0.00005[f]	0.16, 0.04

[a] In toluene (ref 38). [b] In toluene (this work). [c] In CH_2Cl_2 (ref 37). [d] In THF (ref 39). [e] In EC film (ref 21). [f] In EC film (this work).

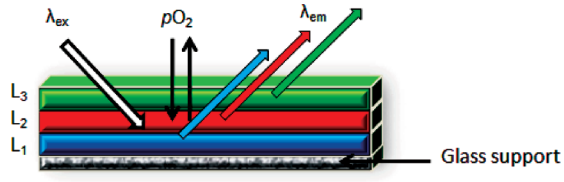

FIGURE 2. Schematic representation of the three-lumophore multilayer oxygen sensors prepared in this study.

previously derived by us to predict the color space response of hypothetical multilumophore colorimetric oxygen sensors (32), and show that there is good agreement between the experimental and modeled color space response of these multilumophore sensors. Finally, we discuss the practical considerations that must be taken into account when preparing multilumophore devices and consider the crucial design factors that must be controlled to avoid discrepancies between the predicted and observed sensor responses.

EXPERIMENTAL SECTION

Materials. Structures of the lumophores used are shown in Figure 1, and their relevant emission properties are summarized in Table 1. Platinum and palladium octaethyporphyrin (PtOEP and PdOEP, respectively) were purchased from Porphyrin Products (Frontier Scientific Ltd., Logan, UT). Chloro-1,3,5-tris(2-pyridyl)benzylplatinum(II) (Ptpyr) was a gift from Dr. J. A. G. Williams and D. L. Rochester (Department of Chemistry, University of Durham, Durham, U.K.) and was used as received. Coumarin 110 (C110), ethyl cellulose (EC; 48% ethoxy content), and poly(vinyl chloride) (PVC; MW = 95 000 g mol^{-1}) were purchased from Aldrich. All solvents were at least AnalaR grade (Fisher Scientific). O_2 and N_2 were BOC "high-purity" gases and were used as received.

Preparation of Multilumophore Oxygen Sensors. The general composition of the multilumophore oxygen-sensing devices described in this work is a series of polymer-encapsulated lumophore layers spin-coated onto a glass support (Figure 2). The lumophore concentration, the polymer identity, and the film thicknesses were varied to change the sensor response. The general methods used to prepare the polymer/lumophore layers

Table 2. Sensor Film Formulations and Relative Contributions of Each Lumophore Layer to the Total Sensor Emission in the Absence of Oxygen

sensor	L_1[a]	L_2[a]	L_3[a]	R^0(B)[b]	R^0(G)[b]	R^0(R)[b]
RG1	PtOEP/EC	Ptpyr/EC			0.062	0.938
RG2	PtOEP/EC	Ptpyr/EC			0.102	0.898
RG3	PtOEP/EC	Ptpyr/EC			0.029	0.971
RG4	PtOEP/PVC	Ptpyr/EC			0.163	0.837
RG5	PdOEP/EC	Ptpyr/EC			0.037	0.963
RB1	C110/PVC	PdOEP/EC		0.025		0.975
RB2	C110/PVC	PdOEP/PVC		0.018		0.982
RGB1	C110/PVC	PdOEP/EC	Ptpyr/EC	0.004	0.126	0.869
RGB2	C110/PVC	PdOEP/EC	Ptpyr/EC	0.047	0.219	0.733
RGB3	C110/PVC	PdOEP/EC	Ptpyr/EC	0.063	0.169	0.767
RGB4	C110/PVC	PdOEP/EC	Ptpyr/EC	0.076	0.083	0.840

[a] L_x indicates the lumophore layer, and the subscript denotes the order the layer was cast onto the support. [b] R^0(B), R^0(G), and R^0(R) correspond to the integrated emission intensity of the B ($\Delta\lambda$ = 380−460 nm), G ($\Delta\lambda$ = 460−580 nm), and R ($\Delta\lambda$ = 580−720 nm) emission bands, respectively, in the sensor emission spectrum recorded in the absence of O_2, where the total sensor emission is normalized to 1.

are described below, and the formulation of each sensor is given in Table 2. These formulations gave reproducible results, for sensors prepared both from the same batch and by different workers. Polymer solutions were prepared by dissolving the polymer in an appropriate solvent to give solutions of similar viscosity as follows: 10% (w/v) EC in 80:20 (v/v) toluene/ethanol; 8.8% (w/v) PVC in tetrahydrofuran (THF). Lumophore stock solutions were prepared by dissolving 5 mg of the lumophore in 5 mL of THF, yielding solutions with a concentration of ca. 10^{-3} M. Polymer/lumophore stock solutions were prepared by dissolving 0.2 mL of the lumophore stock solution in 0.2 g of the polymer stock solution. The resulting mixtures were sonicated for 15 min to ensure a homogeneous distribution of the lumophore in the polymer. Sensor films were prepared by spin coating the polymer/lumophore solutions onto a glass support. Following casting of the film, the UV/vis absorbance spectrum

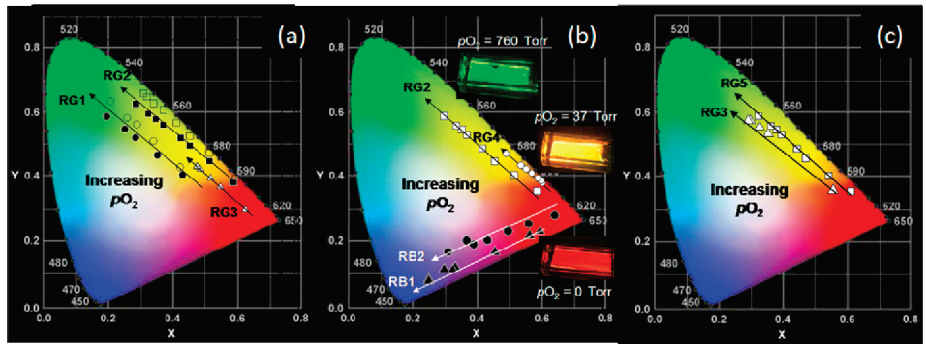

FIGURE 3. CIE *xy* chromaticity diagrams showing the color space response with p_{O_2} for dual-lumophore RG and RB sensors. (a) As a function of R^0(G)/R^0(R): (i) RG1 (circles); (ii) RG2 (squares); (iii) RG3 (triangles). p_{O_2} = 0, 16, 37, 64, and 225 Torr for RG1, and p_{O_2} = 0, 16, 37, 64, 136, 225, 445, and 760 Torr for RG2 and RG3. For sensors RG1 and RG2, the predicted *xy* color coordinates are also shown (open symbols). The *x* coordinates for sensors RG1 and RG3 are shifted by −0.025 and −0.05, respectively, to allow comparison on the same diagram. (b) As a function of the oxygen permeability of the polymer host for the red luomphore: (i) RG2 (squares, EC); (ii) RG4 (circles, PVC); (iii) RB1 (black triangles, EC); (iv) RB2 (black circles, PVC). The *x* coordinates for sensor RG2 are shifted by −0.025 to allow comparison on the same diagram. The *y* coordinates for sensor RB2 are shifted by +0.05 to allow comparison on the same diagram. p_{O_2} = 0, 16, 64, 136, 225, 445, and 760 Torr. The observed sensor response for RG2 at different p_{O_2} values is shown around the edge of the diagram (photographs taken with a Nikon Coolpix 3700 digital camera). (c) As a function of the oxygen quenching efficiency of the red lumophore: (i) RG3 (triangles, R = PtOEP); (ii) RG5 (squares, R = PdOEP). p_{O_2} = 0, 37, 80, 225, 477, and 760 Torr. The *x* coordinates for sensor RG3 are shifted by −0.05 to allow comparison on the same diagram.

was measured and the layer was allowed to dry under air at room temperature for 1 h. Additional layers were then cast on top as required, following the same procedure. L_1 refers to the first layer cast on the glass support, with L_2 and L_3 referring to the second and third cast layers, respectively. By variation of the spin speed used to cast the films, it was possible to control the thickness and therefore the absorbance of each layer. The thickness of the individual polymer film layers was estimated from the film weight and area, using the polymer density (ca. 0.9 g cm^{-3} for EC and ca. 1.4 g cm^{-3} for PVC). Typical film thicknesses were ca. 6 and 8 μm for spin speeds of 4800 and 2500 rpm, respectively.

Instrumentation. UV/vis absorption spectra were measured on a Hewlett-Packard 8452A diode-array spectrometer. Emission spectra were recorded on a Perkin-Elmer MPF-44E fluorescence spectrometer, for which the excitation source was a 150 W xenon arc lamp. The excitation wavelength was 380 nm. Excitation and emission slit widths were 5 and 2 nm, respectively. Emission correction factors for the fluorimeter were obtained using the method of Crosby and Demas (36). Concentrated rhodamine B and methylene blue in ethylene glycol solutions were used as quantum counters for the xenon arc lamp excitation source, which was then reflected from a diffuse-reflectance plate into the emission monochromator of the fluorimeter, to give correction factors between 300 and 700 nm. For wavelengths greater than 700 nm, the manufacturer's photomultiplier response curve was used to provide correction factors. A black filter (0% transmittance at wavelengths >400 nm; 18% transmittance at 380 nm) was placed on the excitation slit to reduce the intensity of scattered visible light. The fluorimeter uses the standard arrangement of excitation and emission axes at 90° to one another. Sensor films were mounted at 24.5° to the excitation beam using a specifically designed slide holder consisting of a sealed triangular unit, two sides of which are fitted with quartz windows for excitation and emission. The slide is immobilized against the third side of the triangle, so that the film is sealed within the holder and the incident light hits the film at an angle of 24.5°. This arrangement means that the excitation light is incident on the top layer first, and light emitted from any layer must pass through overlying layers before detection. The lid of the unit is fitted with two needles to allow a gas stream into the unit and onto the film. Gas mixtures from 0 to 760 Torr (0−100%) O_2 were generated using a gas blender (model no. 852 V1-B, Signal Instruments Co., Surrey, U.K.) with N_2 as the diluent gas. The gas stream of known composition was then passed into the purging chamber of the slide holder, and purging was carried out for 5 min before each measurement to allow equilibration between the gas stream and the sensor. All measurements were carried out at room temperature.

CIE *xy* Color Coordinates. The sensor *XYZ* tristimulus values and *xy* color coordinates were calculated from corrected emission spectra at 5 nm intervals as described previously (32, 35).

RESULTS AND DISCUSSION

Dual-Lumophore RG Sensors. We previously reported a dual-lumophore sensor incorporating PtOEP (red emitter) and Ptpyr (green emitter) as the sensing elements, which exhibits a red−yellow−green "traffic-light" response (31). The p_{O_2} range over which this red−yellow−green color space response is observed depends on three factors: (1) the relative contribution of each lumophore layer to the sensor emission spectrum; (2) the oxygen permeability of each layer; (3) the oxygen quenching efficiency of the red (R) and green (G) lumophores. Figure 3a shows the *xy* color space response of sensors RG1−3 (see Table 2 for formulations) over the range p_{O_2} = 0−760 Torr. Sensors RG1−3 all have the same lumophore combination and polymer support; they vary only in the relative emission contributions of the G and R lumophores, R^0(G)/R^0(R), as determined from the integrated area of the corresponding G and R emission bands in the sensor emission spectrum under N_2 (Table 2). When the R^0(G)/R^0(R) ratio is increased, the initial sensor color in the absence of O_2 shifts from red to orange−yellow on going from RG3 to RG2 to RG1, resulting in a decrease in the lower range of the color space response of the device (Figure 3a). If the R^0(G)/R^0(R) ratio is too low, the upper color response range is also inhibited. This behavior is observed for sensor RG3, where the insufficient contribution from the Ptpyr layer restricts the color space response to the yellow region even at the highest p_{O_2} studied (760 Torr).

The R^0(G)/R^0(R) ratio must therefore be optimized if a device with a color space response spanning the red−yellow−green spectral region is desired. Figure 3a shows

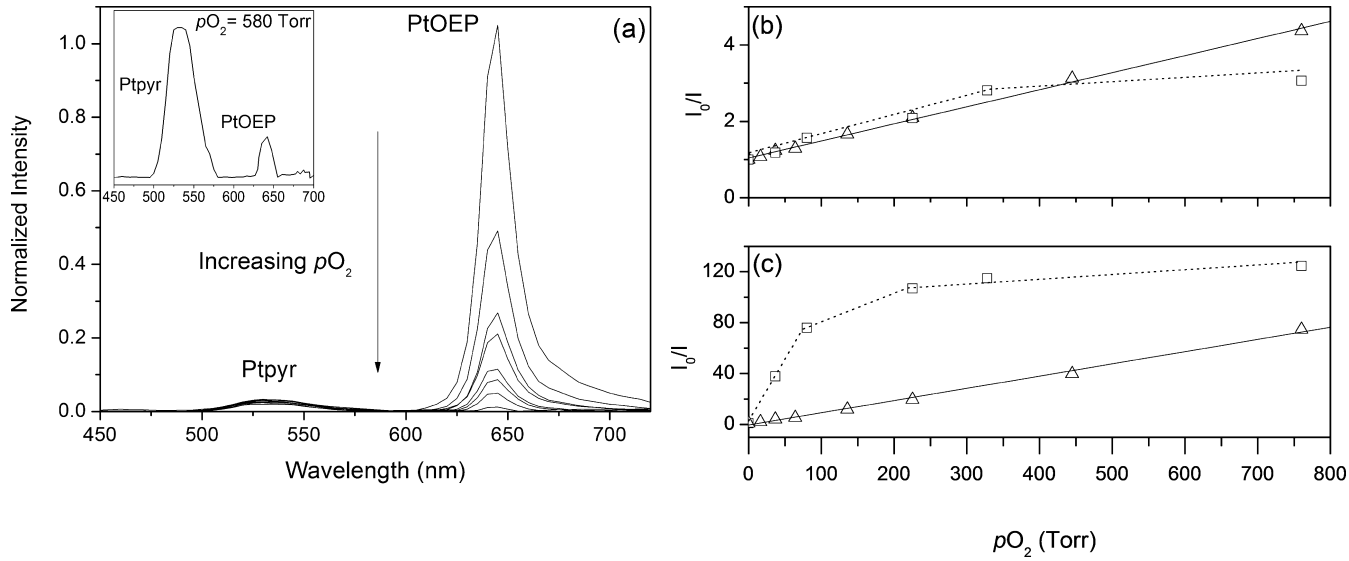

FIGURE 4. (a) Room-temperature emission spectrum (λ_{ex} = 380 nm) of dual-lumophore oxygen sensor RG1 as a function of increasing p_{O_2} (p_{O_2} = 0, 37, 64, 225, 328, 580, and 720 Torr). The inset shows the relative intensity of the Ptpyr and PtOEP emission bands at 580 Torr. Stern–Volmer plots for oxygen quenching of dual-lumophore sensors: (b) quenching of G (Ptpyr) for RG1 (triangles) and RG5 (squares); (c) quenching of R for RG1 (PtOEP, triangles) and RG5 (PdOEP, squares). The solid lines represent a linear fit to the data. The dashed lines serves only as a guide for the eye.

that sensor RG2, with $R^0(G)/R^0(R) \approx 0.11$, best meets these requirements. Sensors RG1 and RG3 exhibit their full color space response potential (orange–yellow–green and red–orange–yellow, respectively) over the limited p_{O_2} range 0–225 Torr; at higher p_{O_2}, no further color change is detected. In contrast, sensor RG2 exhibits its red–yellow–green color response over a much broader p_{O_2} range (0–760 Torr). Thus, by tuning $R^0(G)/R^0(R)$, we can control not only the sensor color space response but also the p_{O_2} range over which the device operates.

The *xy* color space responses of sensors RG2 and RG4 as a function of p_{O_2} are shown in Figure 3b. $R^0(G)/R^0(R)$ values are comparable for these sensors (≈0.1; Table 2), but they differ significantly in the oxygen permeability of the PtOEP host matrix, which is EC for RG2 and PVC for RG4 (P_{O_2} = 11.0×10^{13} and 0.34×10^{13} cm^3 (STP) cm^2 s cm Hg for EC and PVC, respectively) (40). Over the range p_{O_2} = 0–760 Torr, RG2 exhibits a full red–orange–yellow–green color response, while the RG4 response is restricted to red–orange–yellow. The lower oxygen permeability of the PVC layer in RG4 prevents sufficient quenching of the red lumophore layer to drive the sensor color space response into the green spectral region over the p_{O_2} range studied. However, at higher p_{O_2}, it is expected that this sensor should achieve a full red–orange–yellow–green color response. Thus, for low, or ambient, pressure-sensing applications, the oxygen permeability of the red lumophore host layer should be high, while for high pressure sensing, a low permeability host is desirable.

The oxygen quenching efficiency of any layer may also be controlled by using lumophores with different emission lifetimes, τ. Figure 3c shows the *xy* color space response for sensors RG3 and RG5, for which $R^0(G)/R^0(R)$ values are comparable (≈0.03; Table 2) and the polymer host is the same (EC) but for which the red lumophore is either PtOEP or PdOEP, respectively. The color space response is controlled by the low G contribution, which restricts the response to red–orange–yellow over the p_{O_2} range considered (0–760 Torr). The p_{O_2} range over which this transition occurs is, however, controlled by the relative quenching efficiency of the R layer. The emission lifetime of PdOEP is significantly longer than PtOEP ($\tau \approx$ 990 and 100 μs, respectively), and consequently, PdOEP is more efficiently quenched by oxygen. Thus, the color response of RG5 is driven into the yellow spectral region at fairly low oxygen pressures (p_{O_2} = 16 Torr), whereas a pressure of p_{O_2} = 225 Torr is required to produce a comparable response for the RG3 sensor.

Dual-Lumophore RB Sensors. A dual-lumophore sensor exhibiting a red–blue color space response may be prepared by substituting the green anchor lumophore with a blue-emitting lumophore, B, that is also less susceptible to oxygen quenching than the red lumophore layer. The color space responses of two red–blue sensors, RB1 and RB2, as a function of p_{O_2} are shown in Figure 3b. In these sensors, the red lumophore is PdOEP, the blue lumophore is C110, and the sensor color response runs across the red–purple–blue region. The relative luminescence contributions of the blue and red lumophores, $R^0(B)/R^0(R)$, are comparable for sensors RB1 and RB2 ($R^0(B)/R^0(R) \approx 0.02$; Table 2). However, the red lumophore is immobilized in EC and PVC, respectively, for RB1 and RB2 (C110 is immobilized in PVC in both cases). Thus, over the range p_{O_2} = 0–760 Torr, RB1 exhibits a full red–purple–blue color response, while the RB2 sensor is restricted to the red–purple region. Thus, fine-tuning of the sensor response range is obtained by changing the polymer host matrix.

Stern–Volmer Kinetics. Figure 4a shows the emission spectrum of sensor RG1 as a function of p_{O_2}. The luminescence of both the PtOEP and Ptpyr layers is quenched to some extent, with PtOEP emission quenched the most,

as expected on the basis of emission lifetimes ($\tau \approx 100$ and 10 μs for PtOEP and Ptpyr, respectively). At $p_{O_2} = 580$ Torr, the PtOEP emission is almost fully quenched and the green Ptpyr emission predominates (inset, Figure 4a). As was found in previous work with thin film sensors, the equilibrated response times are fast (within less than ca. 30 s to a given p_{O_2} (23)) and in the experimental arrangement used here, which is designed for equilibrium, rather than kinetic studies, the observed response time is more likely limited by gas flow/mixing times than the intrinsic sensor response.

Parts b and c of Figure 4 show the corresponding Stern–Volmer plots obtained for sensors RG1 and RG5. The Stern–Volmer quenching constants (k^{SV}) for sensors RG1–5 are shown in Table S1 (Supporting Information). Linear Stern–Volmer behavior is observed for the quenching of both R and G layers in sensor RG1, while for sensor RG5, a nonlinear quenching dependence is observed with increasing p_{O_2}. Deviations from linearity of Stern–Volmer plots for oxygen quenching are commonly observed for polymer-encapsulated lumophores and are attributed to the lumophore occupying a distribution of sites, which differ in the oxygen diffusion rate or solubility, within the host matrix (7, 21). While the difference in behavior between the palladium and platinum lumophores with respect to linearity of the Stern–Volmer plots is at first glance surprising, it is worth remembering that the oxygen concentration ranges over which this quenching occurs are very different in the two cases, and it may be this, rather than the nature of the metalloporphyrin, that influences the nonlinear Stern–Volmer behavior.

For Stern–Volmer plots exhibiting severe downward curvature, the film sensitivity is often described in terms of $1/S_{50}$, i.e., the reciprocal of p_{O_2} that results in quenching of 50% of the initial luminescence intensity (for linear Stern–Volmer plots, $1/S_{50}$ is equal to k^{SV}) (21). The corresponding $1/S_{50}$ values obtained for the PtOEP/EC layer (RG1) and the PdOEP/EC layer (RG5) are 0.10 and 0.65 Torr^{-1}.

Linear Stern–Volmer intensity plots were obtained for sensors RB1 and RB2 over the p_{O_2} range studied for both the R and B lumophores (Figure S1 in the Supporting Information). Stern–Volmer constants for quenching of PdOEP are $k^{SV} = 0.13$ and 0.04 Torr^{-1} for RB1 and RB2, respectively. This decrease in k^{SV} for PdOEP in RB sensors is probably due to the redissolution of the initially cast C110/PVC layer, L_1, when the second layer is cast, resulting in a "mixed" polymer layer whose oxygen permeability is intermediate to that of the parent polymers. The fact that k^{SV}(PdOEP) values for RB1 and RB2 are of similar orders of magnitude to $1/S_{50}$ for the single PdOEP/PVC film (0.081 Torr^{-1}) (21) supports this idea. This redissolution does not alter the film appearance in any way, and a transparent sensor film is still obtained. However, mixed polymer layers are more likely to result in a significant heterogeneous distribution of lumophore sites, each one having its own associated oxygen quenching kinetics, resulting in the nonlinear Stern–Volmer plots observed for PtOEP and PdOEP.

Extending the Color Space Response. The introduction of a third lumophore may extend both the sensor color space response and the oxygen detection range, introducing the possibility of preparing sensors for applications where a response to a wide range of pressures is required. A multilumophore sensor exhibiting a red–green–blue (RGB) color space response with increasing p_{O_2} should consist of three lumophore layers, which emit individually in the red (R), green (G), and blue (B) regions of the spectrum. In order to drive the sensor color response, the B, G, and R layers must be increasingly susceptible to oxygen quenching. The basic design of the multilumophore RGB sensors described here is a three-layered device consisting of (i) C110/PVC as the blue lumophore in L_1 (closest to the glass support), (ii) PdOEP/PVC as the red lumophore in L_2, and (iii) Ptpyr/EC as the green lumophore in L_3 (Table 2 gives precise formulations).

Figure 5a shows the emission spectrum of sensor RGB2 as a function of p_{O_2}. The luminescence quenching efficiency of each layer is in the order R > G > B. Because of its short lifetime (Table 1) and immobilization in PVC (poor oxygen permeability), quenching of the B lumophore layer is negligible over the p_{O_2} range studied (0–760 Torr). The role of the C110/PVC layer is therefore to act as a blue *anchor* to help drive the sensor color space response. Stern–Volmer plots were obtained for oxygen quenching of all lumophores in RGB devices over the p_{O_2} range studied; the corresponding Stern–Volmer plot for RGB2 is shown in Figure 5b as an example. For sensor RGB2, linear Stern–Volmer plots were obtained for PdOEP and C110, while a slight downward curvature deviation from linearity was observed for oxygen quenching of Ptpyr. The Stern–Volmer constants for quenching of the R, G, and B lumophores in each device are collected in Table S1 (Supporting Information). k^{SV} values for quenching of the blue C110/PVC layer are comparable to k^{SV} obtained for the corresponding single lumophore device (ca. 10^{-5} Torr^{-1}). However, k^{SV} values obtained for quenching of both the R and G lumophore layers are significantly lower than the corresponding reported single-lumophore device sensitivities, indicating that the rate of oxygen quenching of both the R and G lumophores is significantly reduced in these composite sensors, as was previously observed for the dual-lumophore sensors described above.

Figure 6 shows the *xy* color space response with increasing p_{O_2} of some experimental RGB sensors. With just small alterations to the relative contributions of the R, G, and B layers to the total sensor emission, dramatic changes in the sensor color space response are observed. For example, for sensors RGB1 and RGB2, the relative R and G contributions are comparable (Table 2); however, the B lumophore contribution is different, with R^0(B) = 0.004 and 0.047 for RGB1 and RGB2, respectively. The consequence of this change is significant: the color space response of sensor RGB1, with a negligible B contribution, is restricted to the red–yellow–green region, whereas in contrast, sensor RGB2 shows a yellow–turquoise color change over the same p_{O_2} range. The compositions of RGB2 and RGB3 are comparable, but the

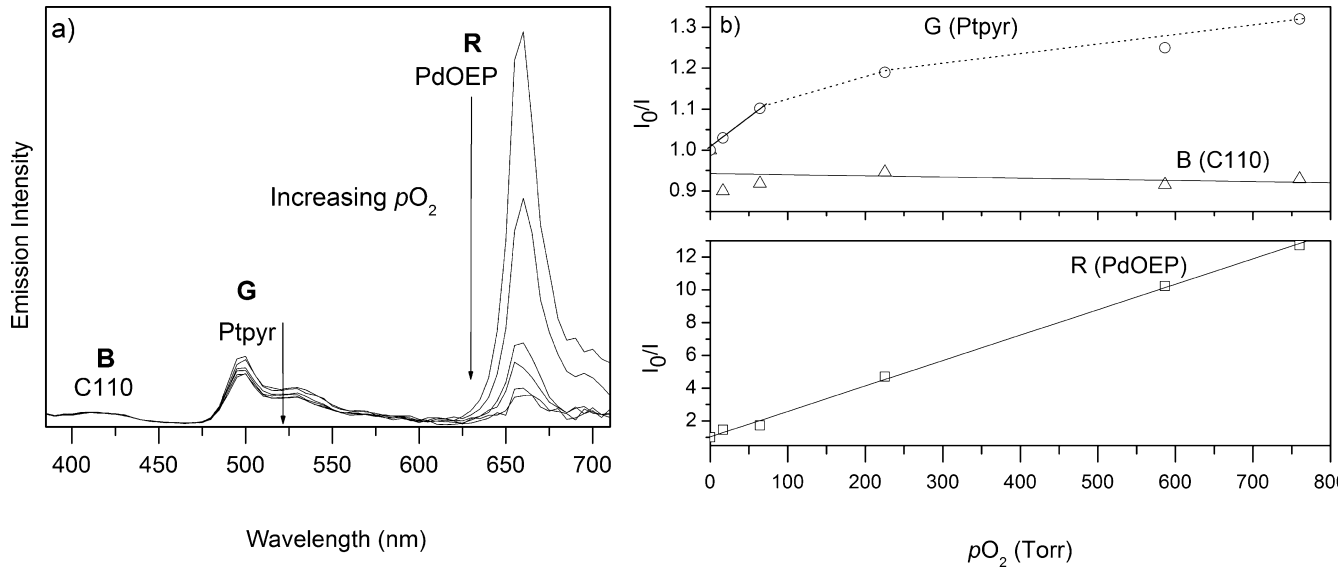

FIGURE 5. (a) Room-temperature emission spectrum (λ_{ex} = 380 nm) of multilumophore oxygen sensor RGB2 as a function of increasing p_{O_2} (p_{O_2} = 0, 64, 225, 328, 586, and 760 Torr). (b) Corresponding Stern–Volmer plots for oxygen quenching of PtOEP, Ptpyr, and C110 for sensor RGB2. The solid lines represent a linear fit to the data. The dashed line serves only as a guide for the eye.

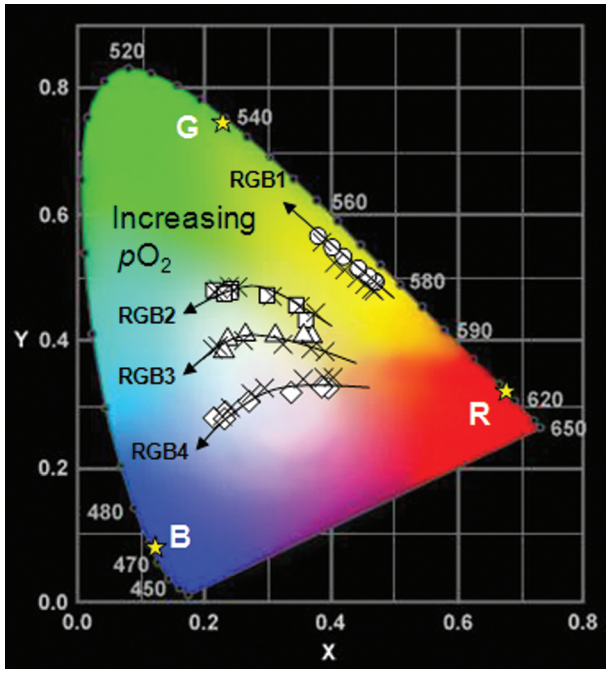

FIGURE 6. CIE *xy* chromaticity diagram showing the color space response with p_{O_2} for multilumophore RGB sensors. The white symbols show the experimental response of the sensors for p_{O_2} = 0, 16, 64, 225, 586, and 760 Torr. The predicted response for each sensor at the same p_{O_2} is shown by the crosses and is determined as described in the text. The arrows serve only to guide the eye.

decrease in the G contribution for RGB3 (R^0(G) ≈ 0.22 and 0.17 for RGB2 and RGB3, respectively) pulls the higher end of the sensor response further into the blue spectral region; i.e., the green response is inhibited. The R contributions for RGB1 and RGB4 are comparable (R^0(R) ≈ 0.8), but the 20-fold increase in the B contribution for RGB4 (R^0(B) ≈ 0.004 and 0.076, respectively), coupled with the low R^0(G), significantly shifts the sensor color response profile from red–green to red–blue over the same p_{O_2}. Thus, the sensor color space response is sensitive to quite small changes in the sensor formulation.

Prediction of the Sensor Color Space Response. It clearly would be advantageous to have some form of preexperimentation sensor design, which allows the color space response of a given sensor formulation to be predicted. We previously reported a mathematical model that enabled the color space responses of some hypothetical multilumophore systems to be predicted in terms of the *xy* color coordinates using Stern–Volmer kinetics to model oxygen quenching of the luminescence (32).

The *xy* color coordinates at any oxygen pressure are given by

$$x = \frac{\sum_{i=1}^{i=n}\left(T_i^0 \frac{1}{1 + k_i^{SV} p_{O_2}} x_i\right)}{T_{sensor}} \qquad y = \frac{\sum_{i=1}^{i=n}\left(T_i^0 \frac{1}{1 + k_i^{SV} p_{O_2}} y_i\right)}{T_{sensor}} \tag{1}$$

where $T_i^0 = X_i + Y_i + Z_i$ for the *i*th layer in the absence of oxygen and *X*, *Y*, and *Z* are the tristimulus values, and T_{sensor} at any oxygen pressure is given by

$$T_{sensor} = \sum_{i=1}^{i=n}\left(T_i^0 \frac{1}{1 + k_i^{SV} p_{O_2}}\right) \tag{2}$$

The relationship between the individual lumophore emission spectrum, *E*, and the total visual response in the absence of oxygen from the layer, T_i^0, can be made using the spectral function, *f*(*E*), which is the sum of the *XYZ* tristimulus values obtained from the emission spectrum for the lumophore normalized to an emission intensity of 1. This, together with the incident light intensity, the fraction of incident light absorbed, and the quantum yield, gives

$$T_i^0 = I_{ex}\left(\frac{1}{10^{\sum_{m=i+1}^{m=n}\epsilon_m c_m l_m}}\right)\left(1 - \frac{1}{10^{\varepsilon_i c_i l_i}}\right)\Phi_i f(E)_i \qquad (3)$$

where ϵ, c, and l are respectively the molar extinction coefficient at the excitation wavelength, lumophore concentration, and film thickness of the ith lumophore layer and I_{ex} is the intensity of the incident excitation source. Φ_i is the emission quantum yield of the ith lumophore in the absence of oxygen. [Since it was necessary to dope the polymer layers with fairly high lumophore concentrations in order to achieve a reasonable sensor response for measurement (optical densities ca. 0.1−0.2), the second term on the right-hand side of eq 3 is necessary to correct for absorption of excitation light by the overlying layers.]

For a sensor for which both the total sensor emission spectrum and the individual lumophore emission spectra are known, the sensor *xy* color space response to oxygen is most easily modeled using a modified version of eq 1, in which T_i^0 for each lumophore layer is replaced by $(R_i^0 f(E)_i)$. The experimental and predicted *xy* color space responses for sensors RG1 and RG2 are shown in Figure 3a (full details of the fitting parameters are given in Table S1 in the Supporting Information). The predicted *xy* coordinates are in generally good agreement with the experimentally obtained values, reproducing the red−yellow−green "traffic-light" response over the p_{O_2} range examined. For both devices, a decrease in the color purity of the experimental sensor response compared to the predicted response is observed, characterized by a shift in the *xy* coordinates away from the spectral locus, toward the center of the diagram. This is most significant at high p_{O_2}, particularly for sensor RG1, where an increasing curvature in the experimental data points is observed. At higher p_{O_2}, the relative emission intensity of both lumophores is decreased by oxygen quenching and the contribution of any background light or scattering in the emission spectrum becomes more significant in the *xy* calculations; we think it may be this that causes the observed decrease in the purity of the sensor color response. It is interesting to consider whether the apparent decrease in spectral purity observed by calculation of the sensor emission as measured using the fluorimeter would also be detected by the human eye. The CIE does not associate a specific color with any point on the *xy* chromaticity diagram because it does not take into account brightness, which is very important in human perception (35). Figure 3b shows the observed sensor film emission colors for RG2 at different O_2 concentrations, which are in good agreement with the hues corresponding to both the experimental and predicted *xy* color coordinates. The predicted *xy* color responses for the RGB sensors are shown in Figure 6 (crossed symbols).

Design Considerations for Multilumophore Colorimetric Sensors. Several additional factors must be considered in relation to sensor design and reproducibility.

1. Reabsorption. Figure 7 shows the absorption spectra of single-lumophore PtOEP, PdOEP, and Ptpyr films and the partial emission spectrum of sensor RGB1 in the absence of O_2, showing the B and G lumophore emissions. All three lumophores absorb to some extent in the region of the C110 emission. Furthermore, PdOEP and PtOEP both exhibit a second reasonably strong absorption band at ca. 530−550 nm, which overlaps with emission from Ptpyr. Although we did not detect any significant problems of reabsorption of emission for the sensors described here, this effect may require consideration when selecting the lumophore combination.

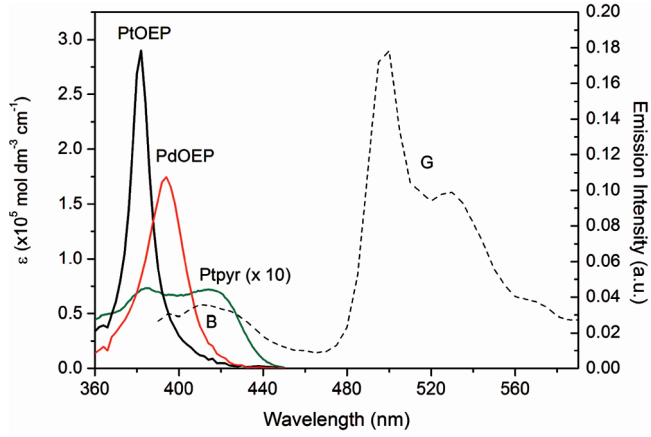

FIGURE 7. UV/vis absorption spectra (shown in terms of the molar extinction coefficient, ϵ) of single-lumophore PtOEP, PdOEP, and Ptpyr films (—) and partial emission spectrum of sensor RGB1 in the absence of O_2 (λ_{ex} = 380 nm) showing emission from C110 (B) and Ptpyr (G). The Ptpyr absorption is magnified 10 times to allow comparison on the same diagram.

2. Deviation from Stern−Volmer Kinetics. For mathematical simplicity, we use Stern−Volmer kinetics to describe oxygen quenching. However, polymer-encapsulated lumophores frequently exhibit complex quenching behavior due to heterogeneity within the host matrix (7, 21) and at least one of the lumophore layers in both RGB1 and RGB4 shows nonlinear Stern−Volmer behavior (Table S1, Supporting Information). Modeling the nonlinear Stern−Volmer luminescence response of polymer-encapsulated lumophores has been the subject of much interest, and a number of mathematical models have been proposed (18, 21, 41). It is probable that by using one of these more sophisticated models, a better match between predicted and experimental responses may be obtained. However, that goes beyond the scope of our work at this time.

3. Formation of "Mixed" Polymer Layers. UV/vis absorption studies have indicated that, during the spin-coating process, previously cast layers redissolve, resulting in the formation of mixed polymer layers. Once completely dry (ca. 24 h), we did not detect any further mixing of the layers. Stern−Volmer analysis suggests that when the polymers in each layer are different, the oxygen permeability of the mixed layer is intermediate to that of the parent polymers. However, the use of individual polymer layers of different oxygen permeabilities in a multilayer device is attractive because it offers the potential to tune the device sensitivity. The prevention of mixed polymer layer formation must therefore be addressed. Possible solutions include the use of different solvents to cast each polymer layer, or alternatively, an approach that we have recently begun to

explore, is the insertion of oxygen-permeable lumophore-free interlayers.

4. Photostability and the Film Deposition Method. Any degradation of the oxygen-sensing component will result in a shift in the color space response. In the presence of oxygen, lumophores may be susceptible to photodegradation by singlet oxygen (20, 29). We have shown that the incorporation of a singlet oxygen scavenger into the sensing layer can significantly improve sensor stability (29), and we are currently extending this approach to multilumophore devices. The use of a polymer as the lumophore host offers the advantage over other matrices, for example, sol–gels, in that inkjet or screen-printing techniques may be used to deposit the sensor layers.

CONCLUSIONS

We have shown that the incorporation of two or more lumophores with different sensitivities and different emission colors in a single sensor introduces the possibility of O_2 measurement across a broad range of concentrations using a simple, easily detectable, visual color indication. It has been shown how the sensor color space response and sensitivity are easily manipulated, with changes to the lumophore identity, concentration, or host matrix having major effects. Thus, it is possible to optimize these sensors for operation over a specific oxygen concentration range and color space. We have demonstrated specific examples of multilumophore sensors exhibiting red–green, red–blue, and red–green–blue color responses and have shown that the *xy* color space response predicted using our previously described model (32) is in good agreement with the observed sensor responses. We have also identified several factors that may be important considerations for sensor design and reproducibility, including the reabsorption of emission between layers, deviation from Stern–Volmer quenching kinetics, and the formation of mixed polymer layers in the spin-coating process.

The possibility of fine-tuning the sensor response using multiple lumophore/polymer layers to give a specific sensitivity and color space profile means that such sensors can, if required, be readily optimized for very specific applications. Moreover, the facility to calculate the color response of a multilumophore sensor using *xy* coordinates prior to experimentation provides a useful design tool. Finally, we note that, in practical terms, it would be possible to provide a visual color calibration strip for any manufactured sensor in which the sensor color response at any p_{O_2} is given, and this can be obtained precisely by direct experimental calibration.

Acknowledgment. R.C.E. acknowledges the University of Wales Swansea for a research studentship. Dr. J. A. G. Williams and D. L. Rochester (Department of Chemistry, University of Durham, Durham, U.K.) are thanked for the generous gift of Ptpyr.

Supporting Information Available: Experimental and calculated data used to model the sensor color space response (Table S1) and supporting Figure S1. This material is available free of charge via the Internet at http://pubs.acs.org.

REFERENCES AND NOTES

(1) Zhao, Y. D.; Richman, A.; Storey, C.; Radford, N. B.; Pantano, P. *Anal. Chem.* **1999**, *71*, 3887.
(2) Park, E. J.; Reid, K. R.; Tang, W.; Kennedy, R. T.; Kopelman, R. *J. Mater. Chem.* **2005**, *15*, 2913.
(3) Xin, L. L.; Wang, X. D.; Guo, G. M.; Wang, X. R.; Chen, X. *Meas. Sci. Technol.* **2007**, *18*, 2878.
(4) O'Mahony, F. C.; O'Riordan, T. C.; Papakovskaia, N.; Kerry, J. P.; Papkovsky, D. B. *Food Control* **2006**, *17*, 286.
(5) Mills, A. *Chem. Soc. Rev.* **2005**, *34*, 1003.
(6) O'Mahony, F. C.; O'Riordan, T. C.; Papakovskaia, N.; Ogurstov, V. I.; Kerry, J. P.; Papkovsky, D. B. *Packag. Technol. Sci.* **2004**, *17*, 225.
(7) Kavandi, J.; Callis, J. B.; Gouterman, M.; Khalil, G. E.; Wright, D.; Green, E.; Burns, D.; McLachlan, B. *Rev. Sci. Instrum.* **1990**, *61*, 3340.
(8) Gouterman, M.; Callis, J.; Dalton, L.; Khalil, G.; Mebarki, Y.; Cooper, K. R.; Grenier, M. *Meas. Sci. Technol.* **2004**, *15*, 1986.
(9) Köse, M. E.; Carroll, B. F.; Schanze, K. S. *Langmuir* **2005**, *21*, 9110.
(10) Köse, M. E.; Carroll, B. F.; Schanze, K. S. *Langmuir* **2005**, *21*, 9121.
(11) Grenoble, S.; Gouterman, M.; Khalil, G. E.; Callis, J.; Dalton, L. *J. Lumin.* **2005**, *113*, 33.
(12) Kimura, F.; Khalil, G.; Zettsu, N.; Xia, Y.; Callis, J.; Gouterman, M.; Dalton, L.; Dabiri, D.; Rodriguez, M. *Meas. Sci. Technol.* **2006**, *17*, 1254.
(13) Stich, M. I. J.; Nagl, S.; Wolfbeis, O. S.; Henne, U.; Schaeferling, M. *Adv. Funct. Mater.* **2008**, *18*, 1399.
(14) For example, see: Oxysense Inc., 13111 N. Central Expressway, Suite 440, Dallas, TX 75243 (www.oxysense.com).
(15) Han, B.-H.; Manners, I.; Winnik, M. A. *Anal. Chem.* **2005**, *77*, 8075.
(16) Higgins, C.; Wencel, D.; Burke, C. S.; MacCraith, B. D.; McDonagh, C. *Analyst* **2008**, *133*, 241.
(17) Lei, B. F.; Li, B.; Zhang, H.; Lu, S.; Zheng, Z. H.; Li, W. L.; Wang, Y. *Adv. Funct. Mater.* **2006**, *16*, 188.
(18) Carraway, E. R.; Demas, J. N.; DeGraff, B. A.; Bacon, J. R. *Anal. Chem.* **1991**, *63*, 337.
(19) McMurray, H. N.; Douglas, P.; Busa, C.; Garley, M. S. *J. Photochem. Photobiol.* **1994**, *80*, 283.
(20) Palma, A. J.; Lopez-Gonzalez, J.; Asensio, L. J.; Fernandez-Ramos, M. D.; Capitán-Vallvey, L. F. *Sens. Actuators B* **2007**, *121*, 629.
(21) Douglas, P.; Eaton, K. *Sens. Actuators B* **2002**, *82*, 200.
(22) Hartmann, P.; Trettnak, W. *Anal. Chem.* **1996**, *68*, 2615.
(23) Eaton, K.; Douglas, P. *Sens. Actuators B* **2002**, *82*, 94.
(24) Jeronimo, P. C. A.; Araujo, A. N.; Montenegro, M. C. B. S. M. *Talanta* **2007**, *72*, 13.
(25) Turel, M.; Cajlakovic, M.; Austin, E.; Dakin, J. P.; Uray, G.; Lobnik, A. *Sens. Actuators B* **2008**, *131*, 247.
(26) Borisov, S. M.; Klimant, I. *J. Fluoresc.* **2008**, *18*, 581.
(27) Schroder, C. R.; Polerecky, L.; Klimant, I. *Anal. Chem.* **2007**, *79*, 60.
(28) Choudhury, B.; Shinar, R.; Shinar, J. *J. Appl. Phys.* **2004**, *96*, 2949.
(29) Ricketts, S. R.; Douglas, P. *Sens. Actuators B* **2008**, *135*, 46.
(30) Khalil, G. E.; Costin, C.; Crafton, J.; Jones, G.; Grenoble, S.; Gouterman, M.; Callis, J. B.; Dalton, L. R. *Sens. Actuators B* **2004**, *97*, 13.
(31) Evans, R. C.; Douglas, P.; Williams, J. A. G.; Rochester, D. L. *J. Fluoresc.* **2006**, *16*, 201.
(32) Evans, R. C.; Douglas, P. *Anal. Chem.* **2006**, *78*, 5645.
(33) Katoh, R.; Nakamura, M.; Sasaki, Y.; Furube, A.; Yokoyama, T.; Nanjo, H. *Chem. Lett.* **2007**, *36*, 1310.
(34) Wang, X.-D.; Chen, X.; Xie, Z.-X.; Wang, X.-R. *Angew. Chem., Int. Ed.* **2008**, *47*, 7450.
(35) Hunt, R. W. G. *Measuring Colour*; Ellis Horwood: Chichester, U.K.,1991.
(36) Crosby, G. A.; Demas, J. N. *J. Phys. Chem.* **1971**, *75*, 991.
(37) Farley, S. J.; Rochester, D. L.; Thompson, A. L.; Howard, J. A. K.; Williams, J. A. G. *Inorg. Chem.* **2005**, *4*, 9690.
(38) Kalyanasundaram, K. *Photochemistry of polypyridine and porphyrin complexes*; Academic Press: New York, 1992.
(39) Glimsdal, E.; Carlsson, M.; Eliasson, B.; Minaev, B.; Lindgren, M. *J. Phys. Chem. A* **2007**, *111*, 244.
(40) Pauly, S. *Polymer Handbook*, 3rd ed.; Wiley: New York, 1989.
(41) Demas, J. N.; McGraff, B. A. *Sens. Actuators B* **1993**, *11*, 35.

AM900007M